DOI: 10.61782/fa.2025.0895

FORUM ACUSTICUM
EURONOISE 2025

THEORETICAL AND EXPERIMENTAL ANALYSIS OF VIBRO-ACOUSTIC COUPLING AT HIGH LEVELS: APPLICATION TO THE DESIGN OF PASSIVE ABSORBING DEVICES

Rita MOUSSA[1*] **Arthur Givois**[1] **Nicolas Dauchez**[1]

[1] Laboratoire Roberval, Université de Technologie de Compiègne, France

ABSTRACT

Noise mitigation is a challenging societal issue. To overcome the limitations of sound-absorbing materials and classical Tuned Mass Oscillators for broadband low-frequency control, this work proposes the use of nonlinear absorbers, known as Nonlinear Energy Sinks (NES), with stiffness governed by a nonlinear law. The studied NES is a thin viscoelastic rubber membrane. When these systems are coupled to a primary system and excited at a sufficient level to activate their nonlinear behavior, an irreversible energy transfer occurs: energy is transferred from the primary system to the NES, where it is dissipated. This study focuses on using the NES to attenuate the first acoustic mode of a circular duct. Under high acoustic levels, the membrane vibrates with significant displacements, resulting in geometric nonlinearities. The behavior of such absorbers is typically described in the literature with a cubic stiffness. However, experimental results appear to contradict these models. For this reason, this work focuses on incorporating material hyperelasticity in addition to geometric nonlinearities. These absorbers are limited by their high excitation threshold required for activation. To address this limitation, this study proposes adjusting theoretical models with experimental data and conducting a parametric analysis of the membrane to optimize the activation threshold.

**Corresponding author*: rita.moussa@utc.fr.

Keywords: *Noise mitigation, Non linear absorber, energy pumping, low frequency, activation threshold.*

1. INTRODUCTION

Various sound absorption methods exist, such as porous materials and Helmholtz resonators. Porous materials are effective for broadband noise reduction but are limited to mid and high frequencies. On the other hand, Helmholtz resonators can be efficient for low frequencies, but their performance is limited to a narrow band around their resonance frequency. For this reason, nonlinear dynamics suggests that using a nonlinear absorber might be an effective solution for the broadband attenuation of low frequencies. These absorbers, usually characterized by a nonlinear stiffness, are known as Nonlinear Energy Sinks (NES). When these systems are applied to a primary system (PS), whether acoustic or vibratory, and are excited at a sufficiently high level to trigger their nonlinear behavior, an irreversible energy transfer from the PS to the NES occurs. The energy is then dissipated within the absorber. Thanks to their nonlinear behavior, NES are characterized by their variable resonance frequency, presenting a significant advantage compared to classical Tuned Mass Damper (TMD) systems. In other words, they are able to adapt their natural frequency to achieve internal 1:1 resonance with the primary system, which governs energy transfer. However, energy transfer is limited by its high activation threshold [1].

The irreversible energy transfer is known as Energy Pumping or also Targeted Energy Transfer. This phenomenon was introduced for the first time by O. Gendelman and A. Vakakis for vibratory applications in [2]. In the acoustic field, energy pumping was observed ex-

perimentally by B. Cochelin et al. in [3]. For acoustic applications, the absorber consists of a thin viscoelastic rubber membrane vibrating with significant displacements compared to its thickness, leading to geometric nonlinearities. This absorber is often modeled in the literature by a Duffing or cubic oscillator. R. Bellet, in [4], numerically studied the influence of membrane parameters (thickness, radius...) on its activation threshold.

In this work, the acoustic application of the NES is investigated. The studied NES consists of a thin viscoelastic rubber membrane coupled to a circular duct in order to attenuate its first acoustical mode. The first paragraph describes the experimental setup designed to characterize the NES and the energy pumping phenomenon. In the second paragraph, experimental results related to the nonlinear dynamics of the membrane are presented. The third paragraph shows experimental results on the influence of membrane thickness in lowering the activation threshold. In the fourth paragraph, a brief description of the methodology used to incorporate material hyperelasticity into the design model is provided. In fact, hyperelasticity appears to be an important parameter for optimizing the nonlinear absorber design, as experimental measurements show that the tested membrane does not exhibit purely cubic behavior.

2. EXPERIMENTAL SETUP

The experimental bench set up at UTC was inspired by the researches conducted at LMA in Marseille [1, 3, 4]. It is made of wood using a laser-cutting machine, as shown in Fig. 1. The device consists of a 1.3 m duct excited at its first acoustical mode, at 132 Hz, using a loudspeaker placed upstream. The membrane is weakly coupled to the duct through a coupling box. The NES consists of a circular thin stretched membrane, clamped at its edges, as presented in Fig. 2. Three different membrane thicknesses were investigated, as presented in Tab. 1.

Table 1. Table summarizing geometrical parameters of the tested membranes.

Membrane	Thickness (mm)	Radius (cm)
1	0.12	1.7
2	0.2	1.7
3	0.5	1.7

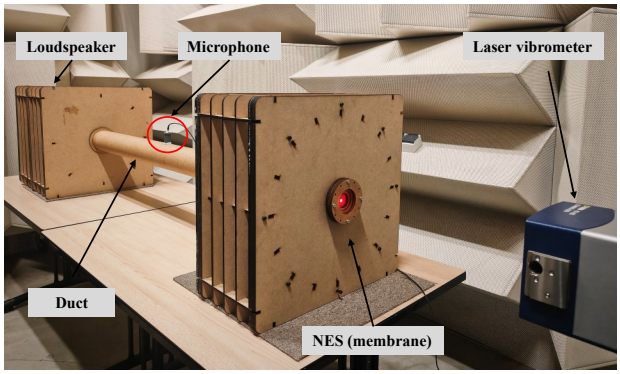

Figure 1. Experimental setup.

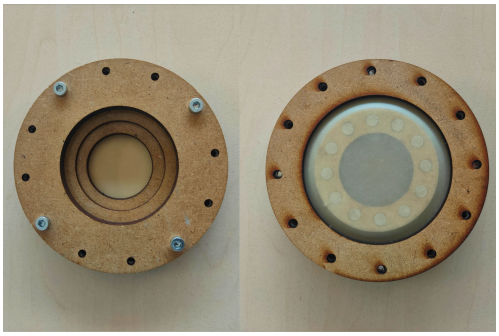

Figure 2. Nonlinear absorber (membrane).

The advantage of this device is that the duct is removable. Indeed, measurements related to energy pumping are performed with the duct mounted. However, to characterize the NES, i.e., the membrane's behavior, its nonlinear dynamics should be studied independently of the PS, therefore, the duct must be removed. Sound pressure is measured using a microphone placed at the center of the duct. On the other hand, a laser vibrometer is used to measure the vibration velocity of the membrane by pointing at its center.

As previously described, NES are efficient above a certain threshold. In order to highlight the efficiency of this absorber in the acoustical field, the frequency response of the duct and the vibrometer velocity are measured before and after the activation of the second membrane of Tab. 1. A current-controlled amplifier is used to adjust the excitation level below and above the activation threshold. As illustrated in Fig. 3, below the activation threshold, for $I = 0.4$ A, the resonance peak of the duct is maximal and the membrane frequency is around 113

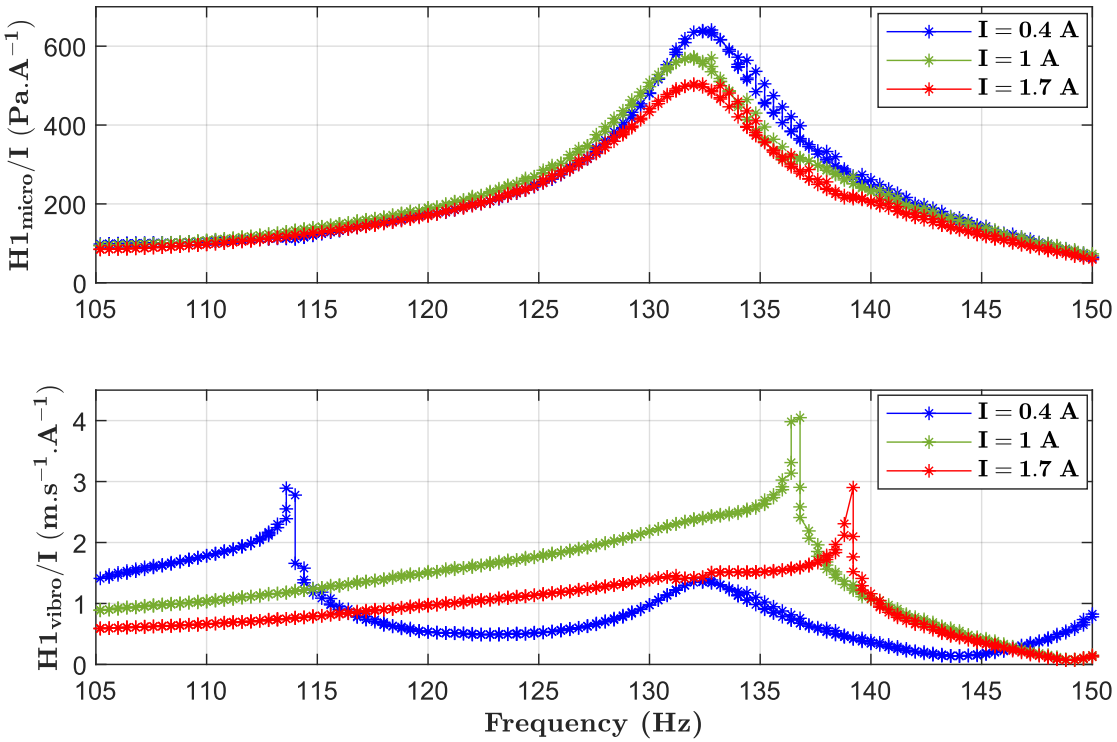

Figure 3. Pressure in the duct and the velocity measured by the vibrometer related to the current intensity feeding the loudspeaker.

Hz. When the current is increased to $I = 1$ A, the membrane is activated and its frequency shifts close to the duct resonance frequency. Energy transfer is then activated, revealing the clipping effect of the peak resonance of the duct. In other words, noise reduction is guaranteed. Similarly, for a higher current value, $I = 1.7$ A, the membrane frequency is placed above the duct's one, and the clipping effect is more pronounced. These results also shed light on the resonance frequency variability of the nonlinear absorber. In addition, Fig. 3 shows a jump at the resonance frequency of the membrane. This phenomenon will be discussed in more detail in Section 3.

3. NONLINEAR DYNAMICS OF THE NES

3.1 Membrane behavior

Measurements without the duct are conducted to characterize the nonlinear behavior of the second membrane of thickness 0.15 mm, as shown in Fig. 4 and illustrated by the schematic in Fig. 5. In this case, the microphone is placed near the membrane inside the coupling box.

As previously introduced, NL absorbers are distinguished by their variable resonance frequency. The backbone curve describes the amplitude/frequency dependence of a nonlinear system in its unforced and undamped state. To experimentally bring the system back to this state, a control loop is applied in order to compensate viscoelastic losses in the membrane through the forcing provided by the loudspeaker.

In the literature, the nonlinear behavior of the NES is described by the Duffing equation, given by the following expression:

$$\ddot{w_m} + \omega_0^2 w_m + 2\xi\omega_0 \dot{w_m} + \Gamma w_m^3 = Q(t), \qquad (1)$$

where w_m is the temporal coordinate of the transverse displacement of the membrane, ξ is the damping coefficient,

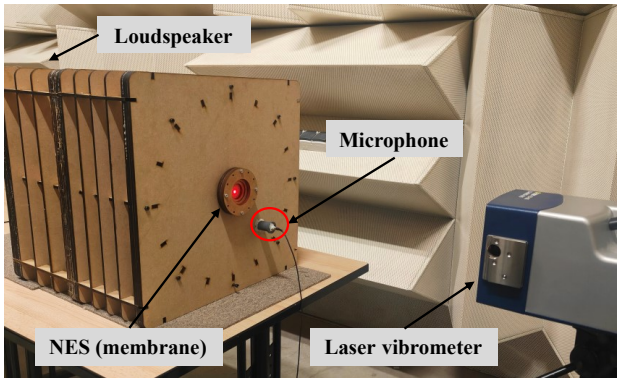

Figure 4. Experimental setup used to measure the membrane's behavior (duct removed).

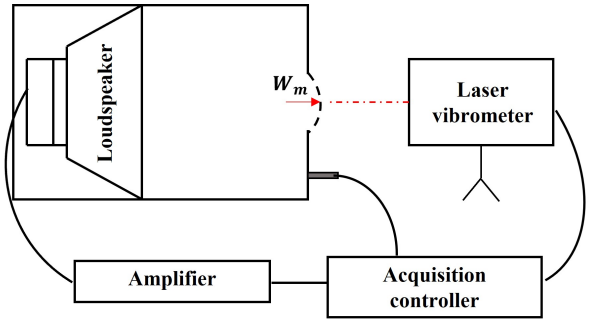

Figure 5. Schematic of the experimental setup used to measure the membrane's behavior.

ω_0 is its angular frequency, Γ is the nonlinear stiffness coefficient and Q is the forcing term resulting from the excitation generated by the loudspeaker.

The harmonic balance method, truncated to its first order approximation, is applied to Eq. (1). Assuming a harmonic excitation, $Q(t)$ is then expressed as a sine forcing, $Q(t) = Q_1 \sin(\Omega t)$. To achieve the unforced and undamped configuration of the system, the membrane displacement w_m is similarly expressed with a phase lag of $\pi/2$ relative to $Q(t)$ as $w_m = w_1 \cos(\Omega t)$. Based on this method and by balancing the sine and cosine components, Eq. (1) can be separated into the following two equations [5]:

$$-\Omega w_1 + \omega_0^2 w_1 + \Gamma w_1^3 = 0, \tag{2}$$

$$2\xi\omega\Omega w_1 = Q_1. \tag{3}$$

In fact, Eq. (2) represents the membrane equation in the absence of external forcing and damping. Eq. (3) expresses the compensation of the membrane's viscoelastic losses through the loudspeaker's forcing. Additionally, it indicates that the phase difference between the velocity measured by the vibrometer and the forcing generated by the loudspeaker should be equal to zero. For this reason, a Phase Lock Loop (PLL) was implemented to maintain phase difference to zero, using VCVrack software. The experimental backbone curve is shown in Fig. 6. In fact, it indicates, for example, that a vibrating velocity of 2.5 m.s^{-1} is required to attenuate a frequency of 130 Hz.

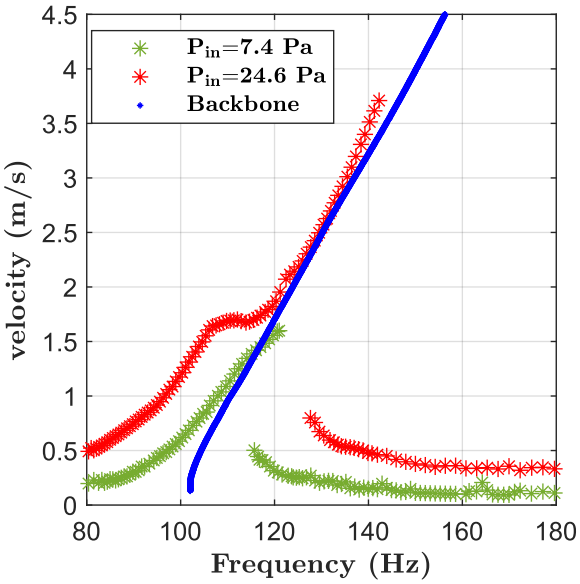

Figure 6. Backbone curve and frequency-response curves of the membrane for different excitation levels. P_{in} denotes the sound pressure level generated by the loudspeaker, related to the forcing term Q in Eq. (1).

Another measurement was conducted to better understand the response curve of the membrane. A frequency sweep was performed while keeping the sound pressure level emitted by the loudspeaker constant. The excitation level was maintained using an integral controller implemented in VCVrack. Two measurements were taken for two different excitation levels, 7.4 Pa and 24.6 Pa. As shown in Fig. 6, the effect of the nonlinearity is to bend the frequency-response curve to the right, indicating a hardening effect of the nonlinearities [6]. Accord-

ingly, the nonlinear coefficient Γ in Eq. (1) has a positive value. In addition, multivalued regions appear. These regions are responsible for the jumping phenomenon as it will be discussed later in section 3.2. Finally, the locus of the peak amplitudes of the frequency-response curves represents the backbone curve.

3.2 Slow Invariant Manifold

In this section, the system's response (PS+NES) in the vicinity of the first acoustical mode of the duct is studied. The amplitude of a harmonic excitation at 132 Hz is gradually increased. The energy transfer from the NES and the duct is called the slow invariant manifold (SIM). Fig. 7 shows the variation of the first harmonic of the pressure measured by the microphone as a function of the first harmonic of the velocity signal measured by the vibrometer. As indicated by the arrows, the excitation level is gradually increased until reaching the NES activation threshold ($1 \rightarrow 2$), where jumping phenomenon occurs. At this point, the NES is activated and the sound pressure level inside the duct decreases suddenly form 223 Pa to 200 Pa, accompanied by an increase of the velocity membrane's vibration velocity from 0.89 m.s^{-1} to 2 m.s^{-1} ($2 \rightarrow 3$). This indicates that the energy has been transferred from the duct and localized in the membrane. The inverse effect occurs when starting at high excitation levels and gradually decreasing the sound pressure level ($5 \rightarrow 6 \rightarrow 7 \rightarrow 8$).

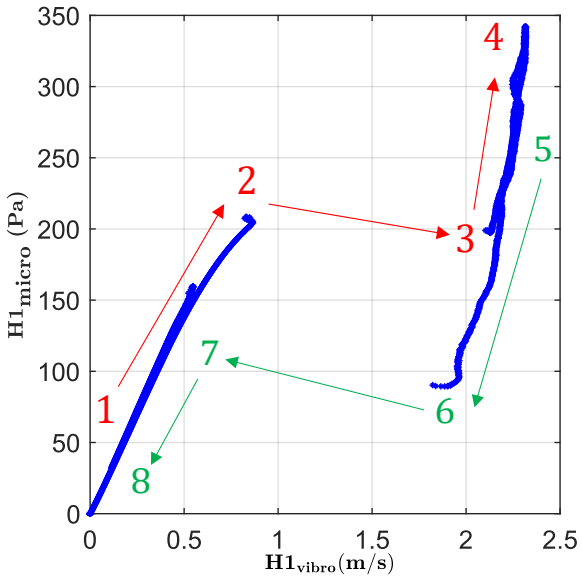

Figure 7. First harmonic of the pressure in the duct versus the first harmonic of the membrane velocity at its center, by varying input forcing at the loudspeaker. This measurement corresponds to the slow invariant manifold (SIM).

4. INFLUENCE OF MEMBRANE THICKNESS

In this section, we investigate how to ensure higher efficiency and a lower activation threshold. In fact, membrane's thickness seems to be a key parameter to investigate. For this reason, backbone curve and SIM measurements were carried out for three different thickness values. The results are presented in Fig. 8 and 9, respectively. It is important to highlight that the difference in sound pressure values between backbone and SIM measurements is due to the microphone placement. Tab. 2 summarizes the results. The attenuation is defined as the sound pressure difference after the jumping phenomenon occurs. In other words, it corresponds to the sudden change in sound pressure level form point 2 to point 3, as indicated in Fig. 7.

In fact, the backbone curves of Fig. 8 show that, to attenuate same frequency-for instance 132 Hz, the required sound pressure level increases with membrane's thickness. On the other hand, Fig. 9 shows that jumping phenomenon or energy transfer from the duct to the NES occurs at lower levels for thinner membranes. In addition, according to the attenuation values presented in Tab. 2, thinner membranes appear to be more efficient, providing greater pressure attenuation.

Table 2. Table summarizing membrane activation thresholds and attenuation for different thicknesses.

Membrane	Threshold (Pa)	Attenuation (Pa)
1	93	33
2	223	23
3	781	25

5. ANALYTICAL MODEL OF THE MEMBRANE

As indicated previously, the membrane is often described in the literature with a cubic behavior. However, the backbone curve in Fig. 6 shows that the vibration amplitude

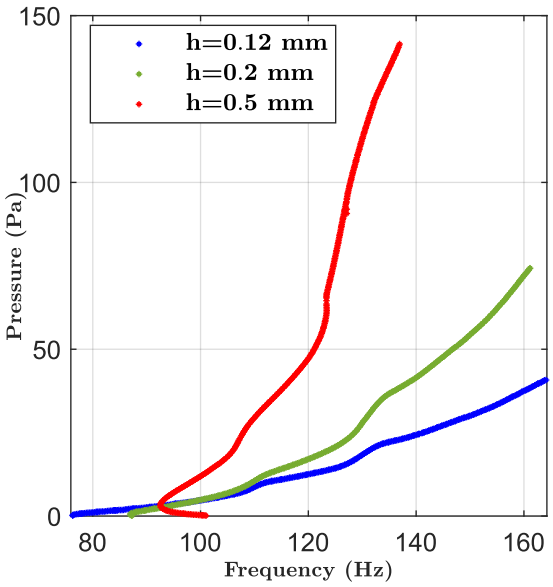

Figure 8. Comparison of backbone curves for different membrane thicknesses.

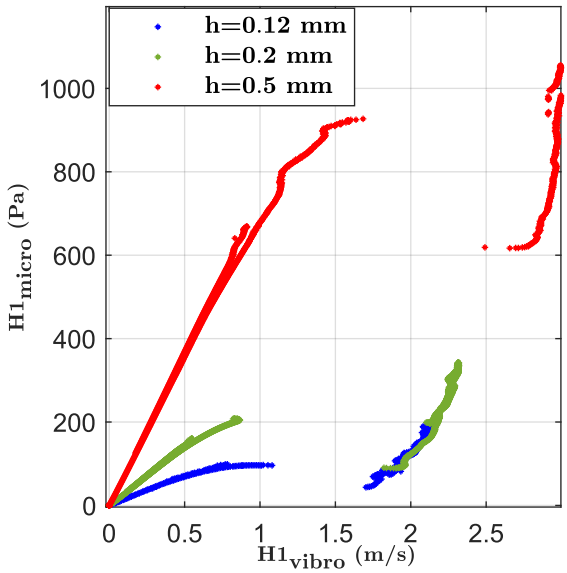

Figure 9. Comparison of slow invariant manifold curves for different membrane thicknesses.

does not vary in a purely cubic manner as a function of frequency. For this reason, considering only geometrical nonlinearities does not appear to be sufficient. This highlights the need to incorporate material hyperelasticity in the membrane model. The methodology used to establish the membrane equation is based on Hamilton's Variational Principle as follows [7]:

$$\delta H = \int_{t_1}^{t_2} \delta L dt = \int_{t_1}^{t_2} \delta(E_c - E_p) dt = 0, \quad (4)$$

where L is the Lagrangian of the system, E_p and E_c are the kinetic and the potential energy respectively and they are expressed as:

$$E_p = \frac{1}{2} \iiint_V W \, dV = \frac{1}{2} \iiint_V \mathbf{S} : \epsilon \, dV, \quad (5)$$

$$E_c = \frac{\rho}{2} \iiint_V (\dot{u}^2 + \dot{w}^2) \, r dr d\theta dz. \quad (6)$$

ρ denotes the material density, while u and w represent the axial and transverse displacements respectively. W is the strain energy density (SED), $\mathbf{S}$ is the second stress tensor of Piola-Kirchhoff, and ϵ is the strain tensor.

Geometric nonlinearities are taken into account based on Von Kármán theory, considering moderate rotations and small strains [8, 9]. This model includes in-plane/transverse coupling. Given the thin structure, the strain tensor elements related to the thickness direction can be neglected, in other words, $\epsilon_{rz} \approx \epsilon_{\theta z} \approx 0$. Only axisymmetric vibrations of the membrane are considered and shear components are neglected. The strain tensor ϵ in cylindrical coordinates is therefore expressed as:

$$\epsilon = \begin{pmatrix} \epsilon_{rr} & 0 & 0 \\ 0 & \epsilon_{\theta\theta} & 0 \\ 0 & 0 & \epsilon_{zz} \end{pmatrix}. \quad (7)$$

According to Kirchhoff-love theory of thin plates, and considering plane stress hypothesis, the stress component S_{zz} is neglected for elastic materials. The strain tensor elements in Eq. (7) are expressed as:

$$\epsilon_{rr} = \frac{\partial u}{\partial r} + \frac{1}{2}\left(\frac{\partial w}{\partial r}\right)^2 \text{ and } \epsilon_{\theta\theta} = \frac{u}{r}. \quad (8)$$

In consequence, the strain energy density for elastic materials is expressed as follows:

$$W = 2\pi \int_0^R \frac{Eh}{2(1-\nu^2)} (\epsilon_{rr}^2 + \epsilon_{\theta\theta}^2 + 2\nu\epsilon_{rr}\epsilon_{\theta\theta}) \, r dr, \quad (9)$$

with ν being the Poisson's ratio assumed to be equal to 0.5 for an incompressible material.

On the other hand, for hyperelastic materials, the transverse contribution of the strain energy density cannot be neglected. To incorporate material hyperelasticity using a Neo-Hookean hyperelastic law, the SED is therefore expressed differently as follows [10]:

$$W = \frac{E}{6}(I_1 - 3), \tag{10}$$

where I_1 is the first invariant of the Cauchy-Green deformation tensor. The Cauchy-Green deformation tensor $\mathbf{C}$ is defined as a function of the Green-Lagrange strain tensor ϵ and the identity matrix $\mathbf{I}$ as $\mathbf{C} = 2\epsilon + \mathbf{I}$. The condition of incompressible material leads to the expression of ϵ_{zz} as a function of ϵ_{rr} and $\epsilon_{\theta\theta}$ in the following form:

$$\epsilon_{zz} = \frac{1}{2(2\epsilon_{rr}+1)(2\epsilon_{\theta\theta}+1)} - \frac{1}{2}. \tag{11}$$

Eq. (10) should be substituted into Eq. (5). Hamilton's Variational Principle is then applied, and the membrane's dynamics are derived while incorporating hyperelasticity. The next step is to decompose the membrane's equation into in-plane and transverse vibrational modes:

$$w(r,t) = \sum_{i=1}^{\infty} \Phi_i(r) q_i(t), \tag{12}$$

$$u(r,t) = \sum_{j=1}^{\infty} \Psi_j(r) \eta_j(t). \tag{13}$$

$\Phi_i(r)$ and $q_i(t)$ are the mode shape and the temporal coordinate of the i^{th} transverse mode. On the other hand, $\Psi_j(r)$ and $\eta_j(t)$ are the mode shape and the temporal coordinate of the j^{th} of in-plane modes. By applying orthogonality properties and reducing the membrane equation to its first transverse mode, we suppose that the resulting membrane equation, incorporating the absorber's geometric and hyperelastic nonlinear coefficients, is written as:

$$\ddot{q_1} + f_d(q_1, \dot{q_1}) + \omega_1^2 q_1 + \Gamma q_1^3 + \alpha q_1^5 = 0, \tag{14}$$

where q_1 denotes the temporal coordinate of the first transverse mode, and ω_1 is its angular frequency. $f_d(q_1, \dot{q_1})$ is the damping function. Γ is the cubic term expressing the geometric nonlinearities and α is the additional nonlinear term induced by the material hyperelasticity. These two coefficients take into account the in-plane/transverse coupling, as they are functions of $\Phi_i(r)$ and $\Psi_j(r)$. Future work consists of evaluating Γ and α and to fit analytical results of equation Eq. (14) with the experimental results of the backbone curve represented in Fig. 6.

6. CONCLUSION

The measurements conducted in this study shed light on the nonlinear behavior of the absorbers. Thanks to their variable natural frequency, they can achieve energy transfer with an acoustic primary system. The nonlinearities of the membrane induce stiffening effects, bending the frequency-response curve. Multivalued regions emerge, leading to a jumping phenomenon that drives energy transfer from the primary system to the NES. When the activation threshold is exceeded, energy pumping occurs, allowing the membrane to capture energy from the duct.

In addition, the membrane thickness appears to be a key parameter to lower the activation threshold and to ensure better attenuation. In the light of this parametric study on the membrane thickness, further parameters as the membrane radius and its viscoelastic losses, will be the subject of future research.

Furthermore, an analytical model incorporating both material hyperelastic nonlinearities and geometric nonlinearities is briefly described. Future works focuses on fitting the analytical model to the measurements for a detailed study of the NES behavior.

7. ACKNOWLEDGMENTS

The authors would like to express their gratitude to Thomas Boutin, head of the design workshop at UTC, for his support and contribution in constructing the experimental setup.

8. REFERENCES

[1] I. Bouzid, *Les absorbeurs dynamiques non linéaires multi-stables*. Marseille: Laboratoire de Mécanique et d'Acoustique, 2023.

[2] O. Gendelman *et al.*, "Energy pumping in nonlinear. mechanical oscillators : Part i—dynamics of the underlying hamiltonian systems," *Journal of Applied Mechanics*, 2001.

[3] B. Cochelin *et al.*, "Experimental evidence of energy pumping in acoustics," *C. R. Mecanique*, p. 639–644, 2006.

[4] R. Bellet, *Vers une nouvelle technique de controle passif du bruit : absorbeur dynamique non linéaire et pompage énergétique*. Université Aix Marseille I, 2010.

[5] V. Denis *et al.*, "Identification of nonlinear modes using phase-locked-loop experimental continuation and normal form," *Mechanical Systems and Signal Processing*, p. 430–452, 2018.

[6] D. T. Mool and A. H. Nayfeh, *Non linear oscillations*. Canada: John Wiley & Sons, INC, 1995.

[7] M. Géradin and D. Rixen, *Théorie des vibrations :application à la dynamique des structures*. Paris: Masson S. A., 1992.

[8] S. Sridhar *et al.*, "Non linear resonances in the forced responses of plates, part i : Symmetric responses of circular plates," *Journal of sound and Vibration*, pp. 359–373, 1975.

[9] M. Monteil, *Comportement vibratoire du steelpan : effet des procédés de fabrication et dynamique non linéaire*. Paris: Ecole Nationale Supérieure de Techniques Avancées ParisTech et Université Pierre et Marie Curie Paris VI, 2013.

[10] I. Breslavsky *et al.*, "Nonlinear vibrations of thin hyperelastic plates," *Journal of sound and Vibration*, p. 1001002, 2014.